

# Effect of Steam Treatment During Plasma Spraying on the Microstructure of Hydroxyapatite Splats and Coatings

H. Li, K.A. Khor, and P. Cheang

(Submitted March 16, 2006; in revised form April 3, 2006)

The major problems with plasma sprayed hydroxyapatite (HA) coatings for hard tissue replacement are severe HA decomposition and insufficient mechanical properties of the coatings. Loss of crystalline HA after the high-temperature spraying is due mainly to the loss of  $\text{OH}^-$  in terms of water. The current study used steam to treat HA droplets and coatings during both in-flight and flattening stages during plasma spraying. The microstructure of the HA coatings and splats was characterized using scanning electron microscope, Raman spectroscopy, Fourier transform IR spectroscopy, and x-ray diffraction. Results showed that a significant increase in crystallinity of the HA coating was achieved through the steam treatment (e.g., from 58 to 79%). In addition, the effects were dependent on particle sizes of the HA feedstock, more increase in crystallinity of the coatings made from smaller powders was revealed. The Raman spectroscopy analyses on the individual splats and coatings indicate that the mechanism involves entrapping of water molecules by the individual HA droplets upon their impingement. It further suggests that the HA decomposition has already taken place before the impingement of the droplets on precoat or substrate. The improvement in crystallinity and phases, for example, from tricalcium phosphate and amorphous calcium phosphate to HA, was achieved by reversing the HA decomposition through providing extra  $\text{OH}^-$ . Furthermore, the steam treatment during the spraying also accounts for remarkably increased adhesion strength from 9.09 to 23.13 MPa. The in vitro testing through immersing the HA coatings in simulated body fluid gives further evidence that the economic and simple steam treatment is promising in improving HA coating structure.

**Keywords** crystallinity, hydroxyapatite, plasma spray, steam treatment

## 1. Introduction

Plasma sprayed hydroxyapatite (HA) coatings on metallic alloy substrates have been successfully used in orthopedic surgery. Both in vitro and in vivo results have claimed the required preferable presence of crystalline HA rather than other calcium phosphate (CP) phases, such as tricalcium phosphate (TCP), tetracalcium phosphate (TTCP), CaO, amorphous calcium phosphate (ACP) in the coatings (Ref 1-3). Consequently, for a long-term functional service of the HA coated implant, the HA coating must have certain crystallinity and less of other CP phases apart from HA. However, since plasma spraying, which was most widely used for the coating deposition (Ref 4-6) owing

to its low cost and easy operation, is a high-temperature process, severe HA decomposition is inevitable (Ref 4, 6-9). Even though many attempts have been successful in reversing the decomposition (from TCP et al. to HA) through some processing techniques, such as postspray heat treatment (Ref 10-12), and other methods, for example, spark plasma sintering (Ref 13), the processes are indeed unsatisfactory due to the critical requirement on sample size, sample shape, and economic considerations.

Generally, according to the mechanism of HA decomposition (Ref 14), loss of water is the key reason accounting for the undesirable phase changes of HA during the plasma spraying. It was found that HA gradually releases its  $\text{OH}^-$  ions and transforms into oxyapatite (OHAP) in the temperature range of 1000 to 1360 °C. Above 1360 °C, the OHAP would decompose into TTCP and  $\alpha$ -TCP (Ref 15). It was proposed that the dehydration of HA gives a solid HA-OHAP solution in which chains of  $\text{OH}^-$  might be replaced by chains of  $\text{OH}^-$ ,  $\text{O}^{2-}$ , and vacancies (Ref 16). The leave of  $\text{OH}^-$  groups in terms of water at high temperatures attained by the HA particles leads to lattice changes associated with structure changes (Ref 14). Consequently, the plasma sprayed HA coatings are composed of several CPs with different amounts depending on the extent of the dehydration of HA. Therefore, the possible approaches used for reversing CPs to crystalline HA must involve providing extra water, and hence  $\text{OH}^-$ . Some researchers have reported their findings that postspray steam treatment on the plasma sprayed HA coatings from their surface showed evidence of a significant reversing effect (Ref 17-20). It was believed that oxyapatite remains stable under dry conditions and would readily transform to HA in the pres-

This article was originally published in *Building on 100 Years of Success, Proceedings of the 2006 International Thermal Spray Conference* (Seattle, WA), May 15-18, 2006, B.R. Marple, M.M. Hyland, Y.-Ch. Lau, R.S. Lima, and J. Voyer, Ed., ASM International, Materials Park, OH, 2006.

**H. Li** (Current address: Biology Department, Bldg. 463, 50 Bell Avenue, Brookhaven National Laboratory, Upton, NY 11973) and **K.A. Khor**, School of Mechanical and Aerospace Engineering, Nanyang Technological University, 50 Nanyang Avenue, Singapore 639798, Singapore; and **P. Cheang**, School of Chemical and Biomedical Engineering, Nanyang Technological University, 50 Nanyang Ave., Singapore 639798, Singapore. Contact e-mail: HLI1@bnl.gov.

ence of moisture (Ref 4, 18). It was reported that water vapor treatment pursued under a low temperature, 125 °C, was effective in achieving good crystallization (Ref 17, 20). However, the treatment seemed to be effective only at the coating surface, and the process can lead to a decrease in adhesive strength (Ref 20). Furthermore, since HA decomposition occurs during the high-temperature spraying, uncertainty remains yet if extra steam can prevent the transformation or, alternatively, if steam can reverse the transformation during the coating formation stage. The current study was conducted with an aim to reveal if the steam takes effect on inhibiting/reversing HA decomposition during plasma spraying and how much the effect can be achieved. The microstructure and chemistry of the coatings and individual splats were characterized using scanning electron microscopy (SEM), Raman spectroscopy, x-ray diffraction (XRD), and Fourier transform IR spectroscopy (FTIR).

## 2. Experimental Details

Starting HA powders were made through a wet chemical method subsequently processed by spray drying to obtain near-spherical shape (Ref 21). An additional annealing heat treatment at 900 °C for 1.5 h was conducted to achieve an entire HA crystalline structure. Three categories of the HA powders were investigated in terms of different particle size ranges, less than 25  $\mu\text{m}$ ,  $-75 +45 \mu\text{m}$ , and  $-125 +75 \mu\text{m}$ , as determined through a laser particle size analyzer (Analysette 22, Fritsch GmbH, Idar Oberstein, Germany) after sieving. Commercial titanium alloy Ti-6Al-4V plates were used as the substrate for the deposition of HA splats and coatings. The sizes of the plates were  $60 \times 20 \times 2$  mm in length, width, and thickness, respectively. After the spraying, the plates with coatings deposited on them were cut into three pieces along the length direction using a diamond blade. The subsequent characterization/in-vitro-incubation was conducted using the small samples with  $\sim 20$  mm in length. Polishing was carried out on the substrate surface using 1  $\mu\text{m}$  diamond paste before splat deposition. For the coating deposition, degreasing and grit blasting on the substrate surface was conducted to make the surface clean and coarse. Alumina sand (250  $\mu\text{m}$ ) was used to coarsen the substrate surface. The air pressure for the grit blasting was 4 bar, and the resultant roughness of the substrate surface was around 4.5  $\mu\text{m}$  in  $R_a$ . A 40 kW direct current (DC) plasma spray system (SG-100, Praxair, Danbury, CT) was used in the current study to accomplish the coating/splats deposition. A net energy of 12 kW was used for the spraying of HA. The primary gas and powder carrier gas was argon with the flow rate of 31 L/min for the primary gas and 7 L/min for the carrier gas. Helium was used as the auxiliary gas (23 L/min). The standoff distance between the gun exit and substrate surface was 120 mm and the powder feeding rate was 8 g/min. The coatings for both the structure characterization and the in vitro testing were  $\sim 180 \mu\text{m}$  in thickness. Figure 1 shows the picture of the facility used for the steam treatment and substrate heating during the plasma spraying. A steam generator (F.lli Casoli mod. M-74, Italy) operated at 1.5 kW was used for the steam generation using distilled water. A stable steam with 2 bar ( $\sim 120$  °C) was provided through two separate pipes into the jig (Fig. 1) for the treatment during the spraying. A hot plate (IEC, Australia) was used for substrate preheating and heating during the spraying

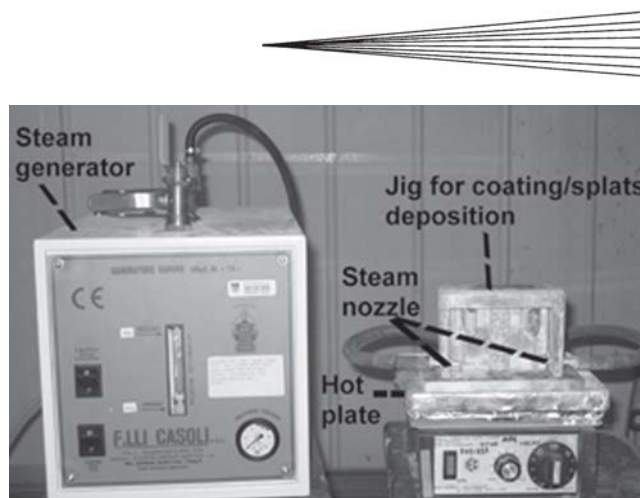


**Fig. 1** Facility setup for the HA coating/splat deposition with water steam treatment

with a fixed temperature of 300 °C. The hot plate was used initially to prevent water droplet formation on the substrate surface since the steam was provided prior to the spraying. As shown in Fig. 1, approximate unique steam supplying was ascertained through using the two-side symmetric steam input. The steam was switched off once the coating/splat deposition was completed. The steam took effect for 50 mm, which means that the distance is 50 mm since the HA droplets start to be accompanying the steam until their impingement. This was achieved through the big jig chamber (50 mm from the substrate surface to the exit of the steam nozzle).

Phase composition of the starting powders and as-sprayed coatings was qualitatively analyzed by means of XRD (MPD 1880, Philips, Eindhoven, the Netherlands). The operating conditions were 40 kV and 30 mA by using Cu-K $\alpha$  radiation. The goniometer was set at a scan rate of 0.02°/s over a  $2\theta$  range of 20 to 60°. The Raman scattering experiments were performed using a Renishaw (Gloucestershire, UK) Raman Imaging Microscop WiRE spectroscopy equipped with 50 mW class 3B helium-neon laser ( $\lambda = 632.816$  nm). The probing spot was about 4  $\mu\text{m}$  in diameter under 1000 $\times$  magnification in an optical transmission light microscope (Leica DML). The Perkin Elmer system 2000 FTIR was used to characterize the samples. The FTIR spectra were obtained with 8 scans per sample over the range of 4000 to 400  $\text{cm}^{-1}$  with a resolution of 4  $\text{cm}^{-1}$ . The microstructure of the coatings and splats was analyzed using scanning electron microscope (SEM, JEOL [Tokyo, Japan] JSM-5600LV).

## 3. Results and Discussion

XRD patterns of the plasma sprayed HA coatings with/without steam treatment are shown in Fig. 2 to 4. The XRD curve of the starting HA powders was also demonstrated (Fig. 3a). It is clear that, as the powder size range is  $-75 +45 \mu\text{m}$ , the steam treated coating shows a higher crystallinity than the coating without steam treatment (increased from 58 to 79%) (Fig. 2). The crystallinity was determined through XRD area integration (using (211) peak of HA). This method has been reported in Ref 22. Figures 3 and 4 further reveal the effect of the steam accompanying the spraying on the phase composition of the HA coatings made from different HA feedstock. As the starting HA powder has a particle size range of  $-125 +75 \mu\text{m}$ , the steam treated

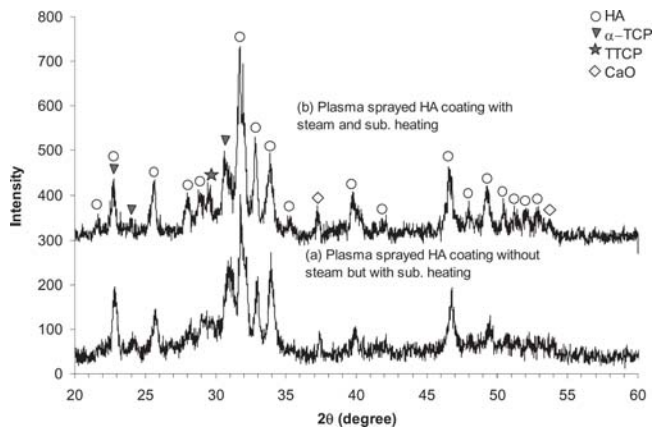


**Fig. 2** XRD patterns of the coatings with/without steam treatment during the spraying indicating an obvious effect of the steam on phase composition of the coatings. The coatings were made from the powders with a particle size of  $-75 + 45 \mu\text{m}$ .

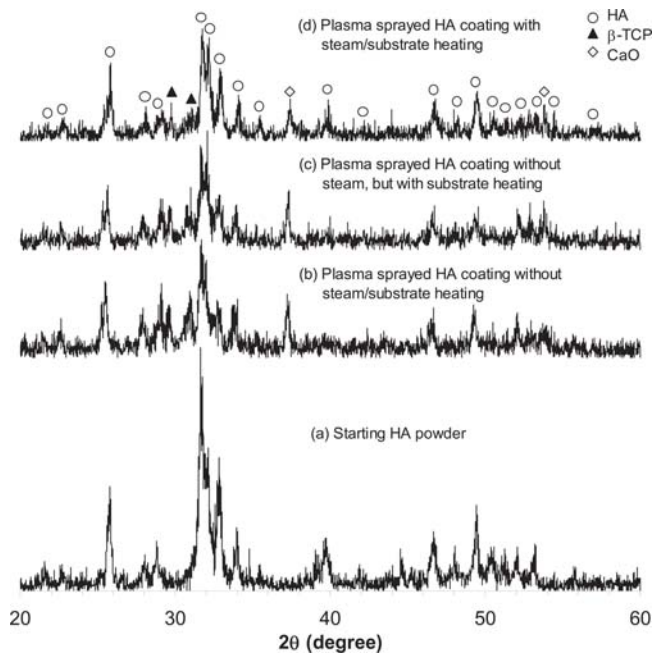


**Fig. 3** XRD curves of the coatings and the starting HA powders ( $-125 + 75 \mu\text{m}$ )

coating also shows less HA decomposition (Fig. 3) as indicated by the relatively low intensity of the peaks assigned to CaO and TCP. This is very promising. From the exclusive investigations on the HA decomposition (Ref 7, 14, 23), it is believed that the transformation is attributed to the high temperature attained by the HA particles during the spraying and their sufficient melt state as this accounts for the formation of ACP upon their impingement and subsequent rapid cooling. As shown in Fig. 3, the coating without substrate heating was also studied to reveal the influence of the substrate temperature on the phase constituents of the coatings. As expected, the substrate heating during the plasma spraying shows minor influence as indicated by the XRD curves (Fig. 3b, c). This, on the other hand, further suggests that

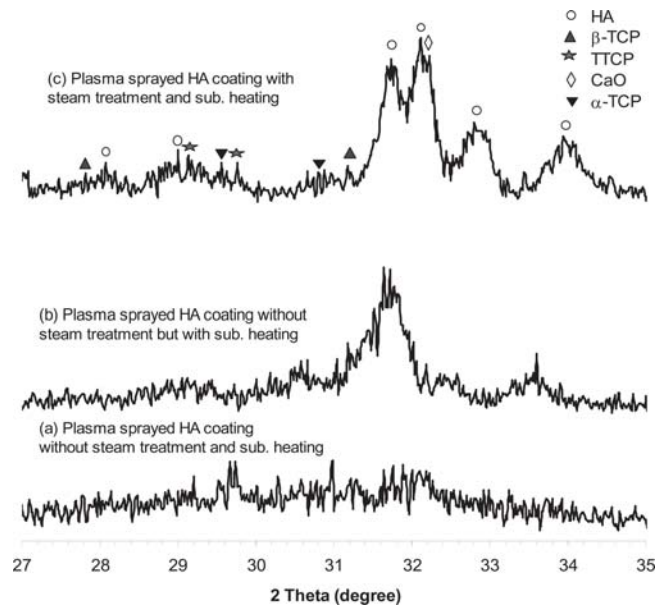


**Fig. 4** XRD patterns of the coatings made with the powders with a particle size of less than  $25 \mu\text{m}$  showing a significant effect of the steam treatment

the influence of the steam on the phases present in the coatings is not caused by the steam temperature ( $\sim 120^\circ\text{C}$ ). For the coatings made from the smallest powders ( $< 25 \mu\text{m}$ ), they show the obvious presence of ACP, CaO, TTCP, and  $\beta$ -TCP apart from HA (Fig. 4). It is not surprising that there is severe phase transformation being observed for these coatings, since smaller HA particles encounter more severe heating due to the overheating state. It is interesting to note that the improvement on the crystallinity by the steam treatment becomes more obvious for these coatings (Fig. 4). The comparison among the coatings made from different HA powders (Fig. 2 to 4) may suggest that the contacting area of the droplets/splats with the steam could play an important role in determining how much the inhibited HA transformation and/or reversed HA decomposition would be achieved. It is clear that smaller HA particles have bigger contacting area with the steam. The mechanism is discussed later in this section.

Raman and FTIR analysis was typically conducted only for the coatings made from large HA particles ( $-75 + 45 \mu\text{m}$ ). For the splats collection, a shielding plate was placed between the substrate and the heating source to filter off individual HA splats and, several holes of 1 mm in diameter were drilled on the plate. For the Raman characterization, the detection was carried out on the surface of individual splats for both the splats and coating samples. It is found that the HA splats demonstrate minor differences in their morphology, which could be due to the full molten state of the particles during the plasma spraying prior to their impingement. The topographical morphology of the individual splats and the splats located at the top layer of the coatings is typically shown in Fig. 5. The Raman spectra of the splats and starting powders are shown in Fig. 6. The Raman curves were taken at the center part, middle part, and surrounding part of the splats. For each type of the splats, three splats were selected for the Raman spectroscopy detection. The results for each type of splat showed very consistent characteristics. For the Raman

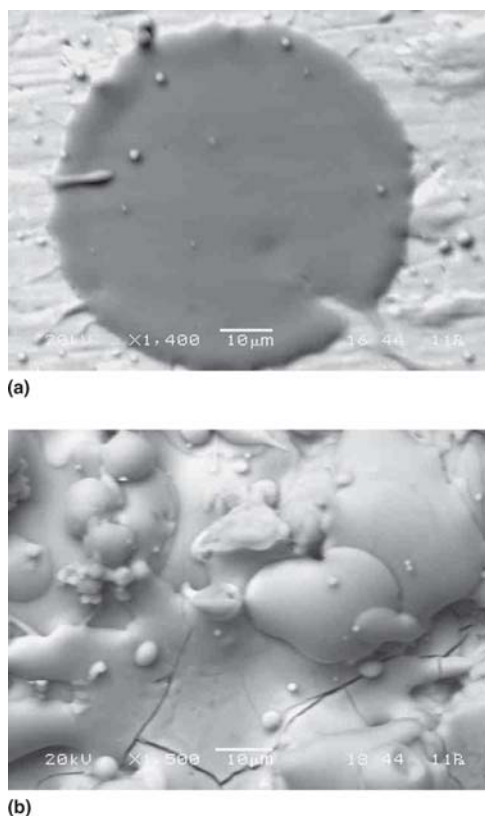


**Fig. 5** Typical topographical SEM morphology of the plasma sprayed HA splats (a) collected on polished Ti6Al4V substrate and (b) located at coating surface

curves, the peaks at  $432(433) \text{ cm}^{-1}$ ,  $453 \text{ cm}^{-1}$ , and  $480 \text{ cm}^{-1}$  are assigned to O–P–O bending mode ( $\nu_2$ ) of the  $\text{PO}_4^{3-}$  group in HA, the peaks at  $588 \text{ cm}^{-1}$ ,  $593 \text{ cm}^{-1}$ ,  $595 \text{ cm}^{-1}$ ,  $603 \text{ cm}^{-1}$ , and  $610 \text{ cm}^{-1}$  refer to O–P–O bending mode ( $\nu_4$ ) of the  $\text{PO}_4^{3-}$  group in HA, the peaks at  $955 \text{ cm}^{-1}$ ,  $956 \text{ cm}^{-1}$ , and  $961 \text{ cm}^{-1}$  are assigned to P–O bond symmetric stretching mode ( $\nu_1$ ) of the tetrahedral  $\text{PO}_4^{3-}$  group in HA, the peaks at  $1037 \text{ cm}^{-1}$ ,  $1047 \text{ cm}^{-1}$ , and  $1076 \text{ cm}^{-1}$  are assigned to P–O bond asymmetric stretching mode ( $\nu_3$ ) of the  $\text{PO}_4^{3-}$  group in HA. It is noted that there is, however, no significant difference among the Raman curves (Fig. 6b to d). The results suggest severe HA decomposition in all these three types of HA splats. This in turn indicates that the phase constituents in the splat with direct contact with the substrate surface might be similar, since the authors' previous study has shown that the Raman analysis is capable of reflecting the phase information of the detected CP splats (Ref 24). The minor difference in the intensity of the  $\nu_1$  peak (Fig. 6d versus Fig. 6b and c) may suggest a transient phase resulted from the steam treatment. Nevertheless, the finding further suggests that the steam has no significant influence on the phase composition of these splats, or even that of the very thin first layer (with the thickness of no more than that of an individual splat).

However, the splats located at the extreme surface of the coatings showed different Raman curves (Fig. 7). The curve for the steam treated HA coating (Fig. 7c) is very similar to that of the starting HA powders (Fig. 6a). This suggests a predominant presence of crystalline HA in the coating. As discussed in the

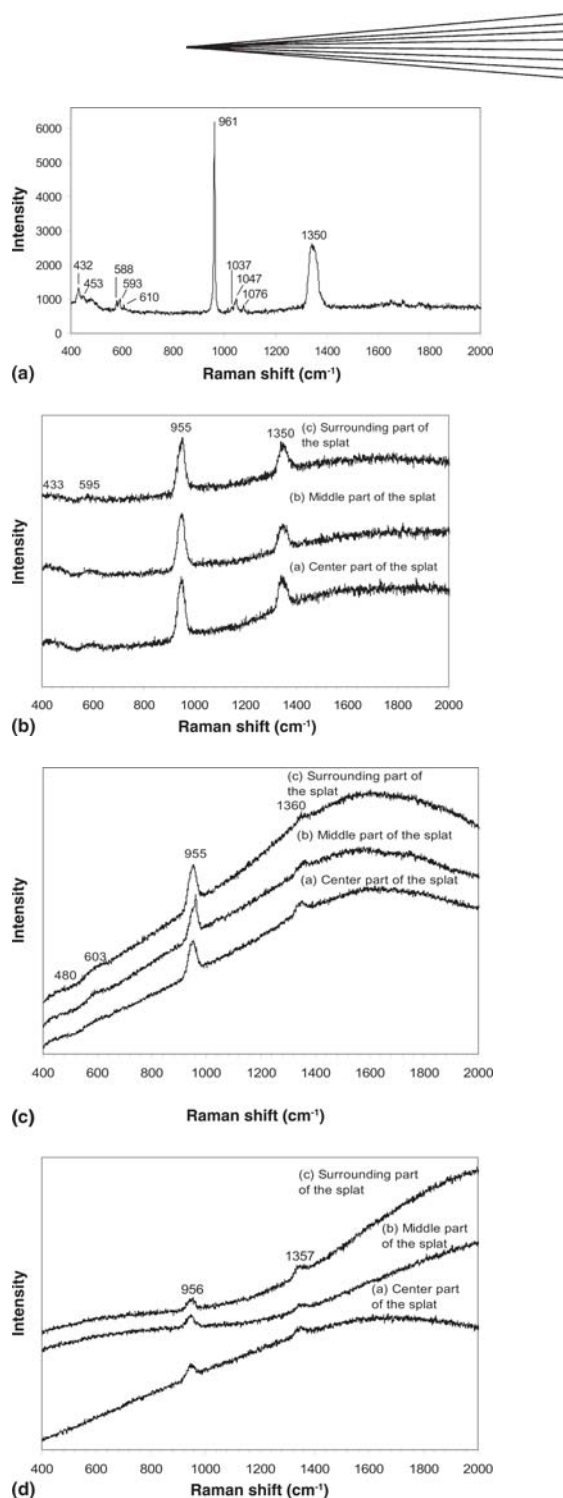


**Fig. 6** Raman spectra detected from surface of the plasma sprayed HA splats (with direct contact with the substrate) with a comparison to that of the starting HA feedstock. (a) Raman spectrum of the starting HA powders. (b) Raman curves of the plasma sprayed HA splat without extra steam treatment and substrate heating. (c) Raman curves of the plasma sprayed HA splat without extra steam treatment but with substrate heating during the spraying. (d) Raman curves of the plasma sprayed HA splat with both steam treatment and substrate heating during the spraying

authors' previous paper (Ref 24), the almost unobservable peaks of  $\nu_3$  ( $\sim 1032$  to  $1081 \text{ cm}^{-1}$ ) on the curve (Fig. 7a and b) are typical features of ACP structure. For the coating deposited

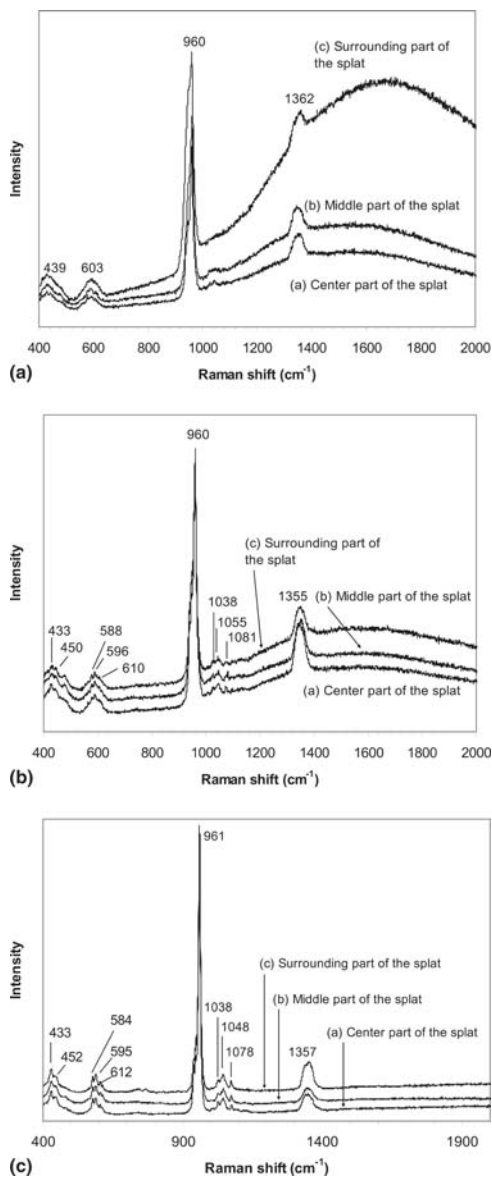


**Fig. 7** Raman spectra detected from typical HA splat located at the HA coating surface, (a) for the coating without steam treatment and substrate heating, (b) for the coating without steam treatment and with substrate heating, and (c) for the coating with steam treatment and substrate heating

without steam/substrate heating (Fig. 7a), the surrounding part of the splat shows a higher amount of ACP than the center of the splat. However, the splat located at the surface of the steam treated coating shows very similar Raman spectra detected from different locations. This suggests the uniform phase constituents within the steam treated splats/coating. The heating of the substrate did show some promising effect on final phases within the coating (Fig. 7b versus Fig. 7a). The Raman results are very consistent with the results revealed through XRD analysis (Fig. 2 and 3).

It is obvious that, based on the comparison among the Raman curves (Fig. 6 b to d), the steam treatment showed minor effect on the phase composition of the splats with direct contact with

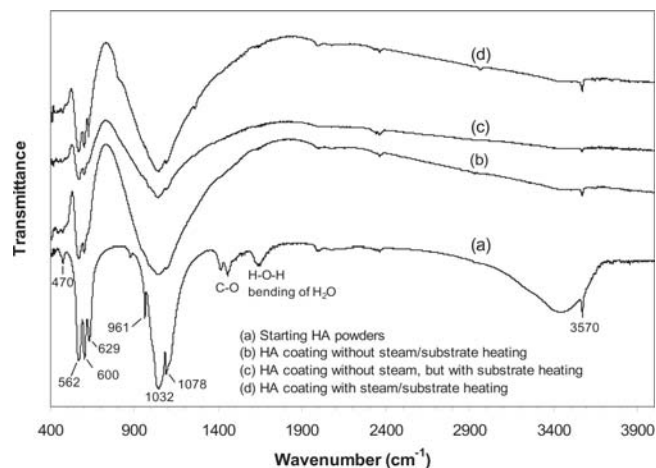


**Fig. 8** IR spectra of the plasma sprayed coatings with a comparison to that of the starting HA powders indicating more amount of crystalline HA in the steam treated HA coatings by the stronger OH<sup>-</sup> peaks than the coatings made without steam treatment

the substrate. However, being consistent with the XRD results, the splats at surface of the coating made with steam treatment show a markedly high crystallinity and less HA decomposition-resulted phases. In the current study, the Raman detection was also conducted at the cross sections of the coatings at different locations, far or near to the coating/substrate interface. The Raman spectra obtained from the second layer (defined here as the layer with one-splat thickness away from the interface) have already shown the similar characteristics to those detected at coating surface. These results further indicate that the significant effect is most probably achieved through entrapping of water molecules during the accumulation of splats resulted from continuous impingement of HA droplets. Furthermore, according to the present observations, it is believed that before the impingement of the HA droplets on pre-coating or substrate, decomposition of HA has already taken place (the extent, of course, depends on the heating extent attained by the particles and the dwelling time of the particles in the plasma torch). The findings fit very well with the discussion made by Gross et al. (Ref 25) that ACP and hydroxylate-deficient oxyapatite form preferably upon rapid cooling, since the Gibbs free energy of HA formation is higher than that of oxyapatite or ACP and, hence, the driving force for nucleation of HA is higher. Another proof that the steam takes effect only at the flattening stage is the formation of microcracks. From the topographical morphology of the coatings, an increased microcrack density was found for the coatings made with steam treatment. These cracks may come from the reversible phase transformation, ACP → HA, TCP → HA, in the presence of water. The restored HA accounts for the formation of some of the microcracks since HA is 3% denser than oxyapatite (Ref 4).

The FTIR results (Fig. 8) further confirm the major findings revealed through XRD and Raman analyses. As shown in Fig. 8, the bands at 3570 cm<sup>-1</sup> and ~629 cm<sup>-1</sup> are attributed to the stretching and flexural modes of hydroxyl (OH<sup>-</sup>) group in HA. They are very sharp (Fig. 8a and d), indicating that the starting powders and the steam treated coating are indeed well crystallized. The peaks labeled at ~562 cm<sup>-1</sup> and ~600 cm<sup>-1</sup> represent

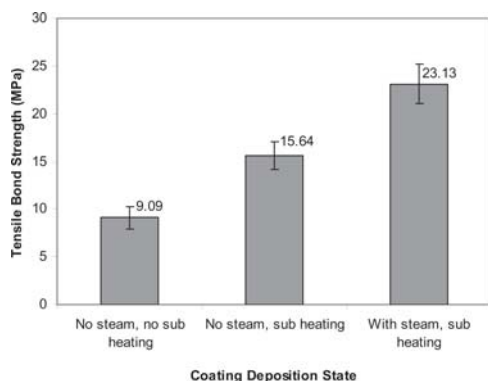
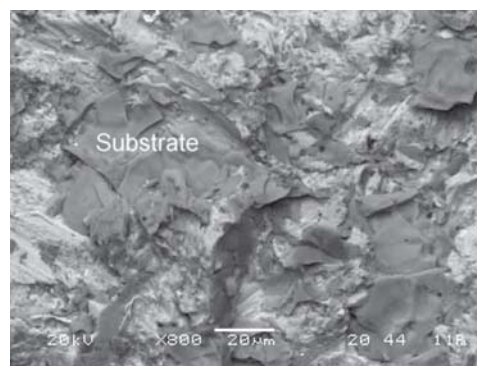


**Fig. 9** Adhesion bonding strength of the plasma sprayed HA coatings made from  $<25\ \mu\text{m}$  powders

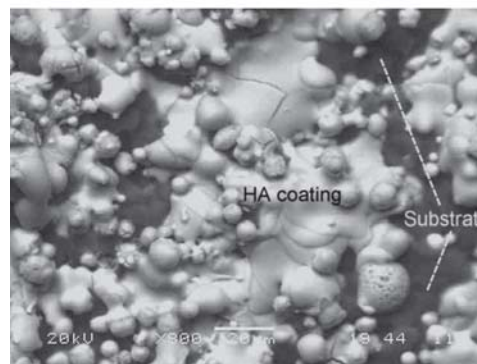
the bending mode  $\text{PO}_4^{3-}$ , and those labeled at  $\sim 961\ \text{cm}^{-1}$ ,  $\sim 1032\ \text{cm}^{-1}$ , and  $\sim 1078\ \text{cm}^{-1}$  are assigned to the stretching vibration mode  $\text{PO}_4^{3-}$ . The weakening of the  $\text{OH}^-$  stretching mode at around  $3570\ \text{cm}^{-1}$  and even disappearance of the flexural mode  $\text{OH}^-$  at  $\sim 629\ \text{cm}^{-1}$  (shown in Fig. 8b and c) suggest the decreased content of crystallized HA in the coatings deposited without water steam treatment.

The adhesion of HA coating plays an important role since loosening of HA coating is very common after implantation. In this study, the adhesive bonding strength of the HA coatings was determined according to the ASTM C 633-79 standard (Ref 26). The coating thickness was  $\sim 200\ \mu\text{m}$ , and the testing was carried out using an Instron universal machine. Since the coatings made from the smallest powders ( $<20\ \mu\text{m}$ ) showed the most promising improvement in coating structure (Fig. 4), the adhesion of these coatings was typically investigated. The results showed that a significant increase of the tensile bond strength, from 9.09 to 23.13 MPa, was achieved through the steam treatment (Fig. 9). To reveal the strengthening mechanism brought about by the steam treatment, the tensile worn surface of the coatings was characterized. It is noted that the failure mode of the coatings is different (Fig. 10). The plasma sprayed HA coating without steam/substrate heating shows a complete adhesive failure mode (fracture at coating/substrate interface), while the coating with substrate heating but without steam treatment shows a mixed failure mode (adhesive/cohesive). The steam treated coating exhibits a complete cohesive failure mode. It indicates that the pre-heating of the substrate is beneficial for a good bonding of the coating, which is probably achieved through decreasing the tensile stress formed after flattening of the droplets. For the steam treated HA coating (Fig. 10c), the fracture within and between splats ( $\sim 50\%$  splat fracture and  $\sim 50\%$  splat detachment) indicates a better mechanical interlocking among the splats than the coatings that did not receive steam treatment. The reason why the steam can significantly improve the bonding state of the coating is yet unclear and needs to be further clarified. It must be noted that the adhesive bonding strength of the coatings made from the finest powders is the lowest among all the current plasma sprayed HA coatings. Nevertheless, the current study gives the evidence of the promising effect of the steam treatment on the adhesion of the coatings.

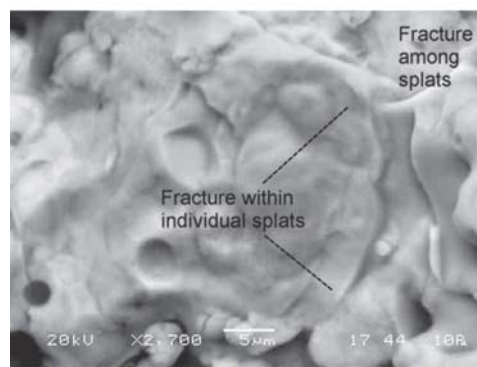
In vitro testing was also carried out through incubating the HA splats and coating samples in simulated body fluid (SBF).



(a)



(b)



(c)

**Fig. 10** SEM morphology of the tensile worn surface of the HA coatings showing (a) a complete adhesive failure for the coating made without steam treatment and substrate heating, (b) a mixed failure mode (cohesive/adhesive) for the coating made with substrate heating, but without steam treatment, and (c) an entire cohesive failure for the coating with steam treatment and substrate heating. The coatings were made from  $<25\ \mu\text{m}$  powders.

The Kokubo solution was used for the testing, and the preparation of the SBF and the testing samples has been described elsewhere (Ref 24, 27). Results showed that the steam treated HA coating exhibited lower dissolution rate than the coating without steam treatment ( $\sim 1$  day delay). It has been clear that the relative dissolution rate can reflect the CP phases present in the samples (Ref 2). The result confirms the findings revealed through XRD, Raman, and FTIR analyses that the steam treated HA coating is composed of more crystalline HA than the coating without

steam treatment. Also, the in vitro incubation of the splats deposited with/without the steam treatment showed consistent results with those reported previously (Ref 24).

#### 4. Conclusions

Water steam was provided accompanying in-flight HA droplets and splats/coating formation during plasma spraying of HA. The steam treatment during the plasma spraying is effective in reversing undesirable phases, ACP (the major effect), TCP, and so forth, to crystalline HA. The mechanism of reversing HA decomposition involves mainly the entrapping of water molecules by individual HA droplets upon their impingement. The present results indicate that the phase changes of HA during plasma spraying has already taken place during in-flight stage of the HA particles. Furthermore, apart from reversing HA decomposition, the steam is also capable of significantly increasing the adhesion strength of the coating with >100% (the coatings were made from <25  $\mu\text{m}$  powders). To provide steam is an easy and economic process during plasma spraying. The major problem with plasma spraying of HA can now be easily solved. The current study is therefore essentially practically valuable. It is also expected that phase composition of the HA coatings can be altered through changing the pressure and flow rate of the steam.

#### Acknowledgment

The author, H. Li, acknowledges the Singapore Millennium Foundation (SMF) for its postdoctoral fellowship.

#### References

1. M. Nagano, T. Nakamura, T. Kokubo, M. Tanahashi, and M. Ogawa, Differences of Bone Bonding Ability and Degradation Behaviour In Vivo between Amorphous Calcium Phosphate and Highly Crystalline Hydroxyapatite Coating, *Biomaterials*, 1996, **17**(18), p 1771-1777
2. P. Ducheyne, S. Radin, and L. King, The Effect of Calcium Phosphate Ceramic Composition and Structure on In Vitro Behaviour: I. Dissolution, *J. Biomed. Mater. Res.*, 1993, **17**(1), p 25-34
3. S. Best, B. Sim, M. Kayser, and S. Downes, The Dependence of Osteoblastic Response on Variations in the Chemical Composition and Physical Properties of Hydroxyapatite, *J. Mater. Sci. Mater. Med.*, 1997, **8**(2), p 97-103
4. K.A. Gross, V. Gross, and C.C. Berndt, Thermal Analysis of Amorphous Phases in Hydroxyapatite Coatings, *J. Am. Ceram. Soc.*, 1998, **81**(1), p 106-112
5. J. Chen, J.G.C. Wolke, and K. de Groot, Microstructure and Crystallinity in Hydroxyapatite Coatings, *Biomaterials*, 1994, **15**(5), p 396-399
6. H. Li, K.A. Khor, and P. Cheang, Thermal Sprayed Hydroxyapatite Splats: Nanostructures, Pore Formation Mechanisms and TEM Characterization, *Biomaterials*, 2004, **25**(17), p 3463-3471
7. K.A. Gross and C.C. Berndt, Thermal Processing of Hydroxyapatite for Coating Production, *J. Biomed. Mater. Res.*, 1998, **39**(4), p 580-587
8. D.M. Liu, H.M. Chou, and J.D. Wu, Plasma-Sprayed Hydroxyapatite Coating: Effect of Different Calcium Phosphate Ceramics, *J. Mater. Sci. Mater. Med.*, 1994, **5**(3), p 147-153
9. M.T. Carayon and J.L. Lacout, Study of the Ca/P Atomic Ratio of the Amorphous Phase in Plasma-Sprayed Hydroxyapatite Coatings, *J. Solid State Chem.*, 2003, **172**(2), p 339-350
10. J. Vogel, C. Russel, and G. Guntheer, Characterization of Plasma-Sprayed Hydroxyapatite by P-MAS-NMR and the Effect of Subsequent Annealing, *J. Mater. Sci. Mater. Med.*, 1996, **7**(8), p 495-499
11. H. Ji and P.M. Marquis, Effect of Heat Treatment on the Microstructure of Plasma-Sprayed Hydroxyapatite Coating, *Biomaterials*, 1993, **14**(1), p 64-68
12. K. van Dijk, H.G. Schaeken, J.G.C. Wolde, and J.A. Jansen, Influence of Annealing Temperature on RF Magnetron Sputtered Calcium Phosphate Coatings, *Biomaterials*, 1996, **17**(4), p 405-410
13. L.G. Yu, K.A. Khor, H. Li, and P. Cheang, Effect of Spark Plasma Sintering on the Microstructure and In Vitro Behavior of Plasma Sprayed HA Coatings, *Biomaterials*, 2003, **24**(16), p 2695-2705
14. H. Aoki, *Medical Applications of Hydroxyapatite*, Ishiyaku EuroAmerica, Inc., Tokyo, St. Louis, 1994
15. C. Liao, F. Lin, K. Chen, and J. Sun, Thermal Decomposition and Reconstitution of Hydroxyapatite in Air Atmosphere, *Biomaterials*, 1999, **20**(19), p 1807-1813
16. R. McPherson, N. Gane, and T.J. Bastow, Structural Characterization of Plasma-Sprayed Hydroxyapatite Coatings, *J. Mater. Sci. Mater. Med.*, 1995, **6**(6), p 327-334
17. M. Shirkanzadeh, X-Ray Diffraction and Fourier Transform Infrared Analysis of Nanophase Apatite Coatings Prepared by Electrocrystallization, *Nanostruct. Mater.*, 1994, **4**, p 677-684
18. K. Yamashita, T. Arashi, K. Kitagaki, S. Yamada, and K. Ogawa, Preparation of Apatite Thin Films Through RF-Sputtering from Calcium Phosphate Glasses, *J. Am. Ceram. Soc.*, 1994, **77**(9), p 2401-2407
19. Y. Cao, J. Weng, J. Chen, J. Feng, Z. Yang, and X. Zhang, Water Vapour-Treated Hydroxyapatite Coatings after Plasma Spraying and Their Characteristics, *Biomaterials*, 1996, **17**(4), p 419-424
20. W. Tong, Z. Yang, X. Zhang, A. Yang, J. Feng, Y. Cao, and J. Chen, Studies on Diffusion Maximum in X-ray Diffraction Patterns of Plasma-Sprayed Hydroxyapatite Coatings, *J. Biomed. Mater. Res.*, 1998, **40**(3), p 407-413
21. S.W.K. Kweh, K.A. Khor, and P. Cheang, Production and Characterization of Hydroxyapatite (HA) Powders, *J. Mater. Proc. Technol.*, 1999, **89-90**, p 373-377
22. H. Li, K.A. Khor, and P. Cheang, Properties of Heat Treated Calcium Phosphate Coatings Deposited by High Velocity Oxy-Fuel (HVOF) Spray, *Biomaterials*, 2002, **23**(10), p 2105-2112
23. M. Ogiso, Y. Yamashita, and T. Matsumoto, Differences in Microstructural Characteristics of Dense HA and HA Coating, *J. Biomed. Mater. Res.*, 1998, **41**(2), p 296-303
24. H. Li, B.S. Ng, K.A. Khor, P. Cheang, and T.W. Clyne, Raman Spectroscopy Determination of Phases within Thermal Sprayed Hydroxyapatite Splats and Subsequent In Vitro Dissolution Examination, *Acta Mater.*, 2004, **52**(2), p 445-453
25. K.A. Gross, C.C. Berndt, and H. Herman, Amorphous Phase Formation in Plasma-Sprayed Hydroxyapatite Coatings, *J. Biomed. Mater. Res.*, 1998, **39**(3), p 407-414
26. "Standard Test Method for Adhesion or Cohesive Strength of Flame-Sprayed Coatings," *Annual Book of ASTM Standard*, ASTM, 1999
27. K.A. Khor, H. Li, P. Cheang, and S.Y. Boey, In Vitro Behavior of HVOF Sprayed Calcium Phosphate Splats and Coatings, *Biomaterials*, 2003, **24**(5), p 723-735